

Experimental Evaluation of Dynamic Redundancy Resolution in a Nonholonomic Wheeled Mobile Manipulator

Glenn D. White, Rajankumar M. Bhatt, *Member, IEEE*, Chin Pei Tang, *Student Member, IEEE*, Venkat N. Krovi, *Member, IEEE*

Abstract—Mobile manipulators derive significant novel capabilities for enhanced interactions with the world by merging mobility with manipulation. However, a careful resolution of the redundancy and active control of the reconfigurability, created by the surplus articulated degrees-of-freedom and actuation, is the key to unlocking this potential. Nonholonomic wheeled mobile manipulators (NH-WMM), formed by mounting manipulator arms on disc-wheeled mobile bases, are a small but important subclass of mobile manipulators. The primary control challenges arise due to the dynamic-level coupling of the nonholonomy of the wheeled mobile bases with the inherent kinematic and actuation redundancy within the articulated-chain. The solution approach in this paper builds upon a dynamically-consistent and decoupled partitioning of the articulated system dynamics between the external (task) space and internal (null) space. The independent controllers, developed within each decoupled space, facilitate active internal reconfiguration in addition to resolving redundancy at the dynamic level. Specifically, two variants of null-space controllers are implemented to improve disturbance-rejection and active reconfiguration during performance of end-effector tasks by a primary end-effector impedance-mode controller. These algorithms are evaluated within an implementation framework that emphasizes both virtual prototyping (VP) and hardware-in-the-loop (HIL) testing with representative case studies.

Index Terms— Nonholonomic wheeled mobile manipulator, dynamic redundancy resolution, virtual prototyping, hardware-in-the-loop

I. INTRODUCTION

THE mobile manipulation paradigm capitalizes on the novel benefits and capabilities created by the addition of mobility to the archetypical fixed base manipulator. Many variants are possible, based on the nature of the mobile base (gantry system, another manipulator or some wheeled or tracked platform) and the nature of the mounted manipulator

(number and actuation of the articulations). Numerous applications [1-8], ranging from gantry-mounted manipulators on the shop floor to highway maintenance robots to robotic earth-moving excavators, have capitalized the expanded workspace (conventional/dexterous), reconfigurability, improved disturbance rejection capabilities and robustness to failure. The challenges, however, arise from the manifestation (and need for resolution) of the redundancy – both kinematic redundancy due to the surplus of articulated degrees of freedom (DOF) than required for the task; as well as actuation redundancy due to the surplus of actuation over the controlled outputs. The challenges come to the forefront especially during dynamic interactions of these mobile manipulators with the environment (e.g. during a painting task) making a dynamic-level redundancy resolution critical.

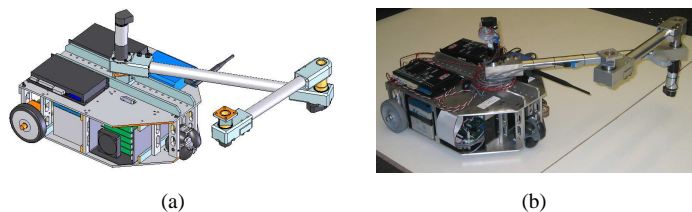


Fig. 1. A nonholonomic wheeled mobile manipulator (NH-WMM): (a) a CAD model, and (b) the corresponding physical prototype.

Our focus is on a subclass of such mobile manipulators called *Nonholonomic Wheeled Mobile Manipulators (NH-WMM)* as shown in Fig. 1. The NH-WMM consists of a wheeled mobile robot (WMR) base with one or more mounted manipulator arms. While robust physical construction makes wheeled bases popular, the kinematics of rolling contact of the various wheel assembly combinations with the terrain creates nonholonomic constraints [9]. The coupling of these nonholonomic constraints with the kinematic/actuation redundancy in a dynamic setting creates interesting control challenges. Our guiding vision is to create and evaluate an overall control framework for such NH-WMM to realize a prioritized satisfaction of its own end-effector interactions. Subsequently, the inherent internal reconfigurability can be exploited to help accommodate, detect and correct for disturbances and maintain a preferred internal configuration when not in conflict with this primary task. Ultimately, such NH-WMM can either autonomously perform or semi-

Manuscript received July 18, 2007, accepted October 17, 2008. This work was supported in part by the National Science Foundation CAREER Award under Grant IIS-0347653.

G. D. White is with General Motors, Honeoye Falls, NY 14472, USA (e-mail: glenn.white@gm.com).

R. M. Bhatt is with Center for Computer Aided Design, University of Iowa, Iowa City, IA 52242, USA (e-mail: rmbhatt@engineering.uiowa.edu).

C. P. Tang and V. N. Krovi are with the Department of Mechanical and Aerospace Engineering, State University of New York at Buffalo, Buffalo, NY 14260 USA (e-mails: nonholonomic@gmail.com, vkrovi@buffalo.edu).

autonomously assist a human operator during dynamic interactions with the world has many applications.

In a redundant manipulator, the determination of the actuator rates/forces for a given end-effector motions/forces is typically an under-constrained problem but essential for motion planning/control. Many schemes have been proposed with an underlying theme of optimizing some measure of performance based on the differential kinematics [10]. For instance, the augmented Jacobian approaches are extended for kinematic redundancy resolution in the case of mobile manipulators by [1, 4]. De Luca et al. [6] recently augmented such Jacobian using the *interaction matrix* from a camera to achieve image-based visual servoing. However, as Wang and Kumar [11] note, if the augmented Jacobian is not the Jacobian of a kinematic function $f(\underline{q})$, the resulting trajectories may not be globally integrable. Alternatively, the decoupled Jacobian approaches, exemplified by Yamamoto and Yun [2] decompose the motions of the mobile manipulator into decoupled WMR and manipulator subsystems. The WMR is then controlled so as to bring the manipulator to a preferred configuration (using criteria such as the manipulability measure) as the end-effector performs a variety of unknown manipulation tasks. The decoupling approach lends itself better to decentralized planning and control of the mobile base and the manipulator arm. Fruchard *et al.* [5] attempted to provide a unified kinematic control framework using the transverse function such that it is independent of the configuration of the mobile base in a WMM system. All the above cases focus on kinematic-level redundancy resolution that implicitly assumes the availability of good rate controlled actuators.

However, our focus in this paper is on dynamic-redundancy resolution within the articulated chain. In exactly-actuated systems, only as many components of the motions/forces as degrees of actuation can be controlled. However, in redundantly actuated systems, it is meaningful to exploit the surplus actuator inputs to achieve secondary goals, in addition to primary task performance. Traditionally, such secondary criteria have included either the contact- or internal-force distribution as seen in multilegged walkers [12], multifingered hands [13], multi-arm systems [14, 15] and parallel manipulators [16]. Fully actuated mobile manipulators have been examined to study of the effect of the dynamic interaction between the manipulators and the mobile platform on the task performance [17]. It is noteworthy that the location of the manipulator arm relative to the mobile base has considerable effect on the performance of a mobile manipulator and needs to be carefully considered [3]. Lew and Moon [18] presents a micro/macro manipulation approach to decouple these systems into fast/slow subsystems to improve the end-effector motion of a compliant base mobile manipulator in the sagittal plane alone. Tan *et al.* [19] controlled a holonomic mobile manipulator to manipulate a passive nonholonomic cart along straight lines, corners or sinusoidal trajectories. Inoue *et al.* [20] considers external force disturbance rejection in the form

of disturbance observer in a NH-WMM, whereas our method has the potential to regulate the end-effector force [21].

The approach adopted in our work is to consider the alternate partitioning of the dynamics into a task/end-effector motion space and an internal/null-motion space. Khatib [22] proposed a method of controlling redundant serial-chain systems by projecting the system dynamics into the task-space to realize an end-effector dynamic model together with a dynamically-consistent actuation that provides decoupled control of joint motions in the null space. Such a partitioning, defined in terms of a metric endowed by the kinetic energy of a simple mechanical system, can formally be shown to be orthogonal and decoupled [23]. This was subsequently extended for mobile manipulator systems with *holonomic* bases [7] and fully actuated manipulators [24]. However, to the best of our knowledge, this has never been extended to and evaluated within experimental NH-WMMs. Realizing control of end-effector motion/force outputs in task-space by the NH-WMMs is a critical precursor to our longer-term goal of decentralized payload manipulation operations [8, 21].

The contribution of this paper comes from the systematic experimental validation of realization of dynamic end-effector interaction control of a NH-WMM with both nonholonomy and redundancy. This is achieved by creating a dynamically-consistent partitioning of motions/forces into decoupled external (task) space and internal (null) space components. By an explicit prioritization, a primary end-effector task-space impedance-mode controller is developed to allow a NH-WMM module to control its end-effector/environment dynamic interactions. The surplus of actuation is used to implement a secondary null-space controller to control internal-reconfigurations that do not conflict with the primary tasks. Emphasis is placed on the development of two variants of null-space controllers (based on the kinematic and dynamic models of WMR), and their performance in terms of input torque profiles on the physical prototype system.

The rest of this paper is organized as follows: Section II briefly reviews the mathematical model of the NH-WMM. Section III develops the decoupled yet dynamically consistent redundancy resolution method. Section IV develops the two variants of the null-space controllers. The virtual prototyping and hardware-in-the-loop experimentation framework is presented in Section V. In Section VI, the framework is used for evaluation of the controller proposed. Section VII concludes the paper with a brief discussion.

II. MODELING OF WHEELED MOBILE MANIPULATOR

We first present the dynamic modeling of the NH-WMM as shown in Fig. 2, focusing primarily on the notation to be used in this paper. We broadly follow the development of the dynamics of the WMR base in [25], which is further extended to the NH-WMM case in [21].

A. Dynamics of the WMR

The WMR subsystem is actuated by two independently driven wheels of radii r located at an equal distance b on

either side of the midline. The wheel axes are collinear and are located at a perpendicular distance d from the center of mass (CM). The other related physical properties and parameters are listed in Table I. The instantaneous WMR configuration can be fully described by the extended set of generalized coordinates $\underline{q}_B^T = [x_c \ y_c \ \phi \ \theta_R \ \theta_L]$, where (x_c, y_c) is the Cartesian coordinates of the CM, ϕ is the orientation of the WMR, and θ_R and θ_L are the angular positions of the right and left wheels, respectively. The system is subjected to three nonholonomic constraints of:

$$A_B \dot{\underline{q}}_B = \underline{0} \quad (1)$$

By taking the independent joint velocities $\underline{\nu}_B^T = [\dot{\theta}_R \ \dot{\theta}_L]$, the corresponding null-space matrix that annihilates the constraint matrix can be determined as:

$$\dot{\underline{q}}_B = S_B \underline{\nu}_B \quad (2)$$

This is valid for the case when the wheels are not slipping or skidding, as in [26]. We define a look-ahead point P_a with Cartesian coordinates:

$$\underline{x}_B = (x_a, y_a) = (x_c + L_a C_\phi, y_c + L_a S_\phi) \quad (3)$$

where $S_\phi = \sin \phi$, $C_\phi = \cos \phi$, L_a is the distance from the CM to P_a . The corresponding Jacobian that relates independent joint velocities to velocity of the look-ahead point can be determined as:

$$\dot{\underline{x}}_B = J_B \underline{\nu}_B \quad \text{and} \quad J_B = \frac{r}{2b} \begin{bmatrix} bC_\phi - L_d S_\phi & bC_\phi + L_d S_\phi \\ bS_\phi + L_d C_\phi & bS_\phi - L_d C_\phi \end{bmatrix} \quad (4)$$

where $L_d = d + L_a$. The WMR is actuated by the torques provided from the right (τ_R) and left wheels (τ_L), $\underline{\tau}_B^T = [\tau_R \ \tau_L]$. With the help of the null-space matrix (2), the *projected reduced dynamics* of the WMR can be expressed as [25]:

$$H_B(\underline{q}_B) \dot{\underline{\nu}}_B + \underline{c}_B(\underline{q}_B, \underline{\nu}_B) = E_B(\underline{q}_B) \underline{\tau}_B \quad (5)$$

where H_B is the configuration dependent inertial matrix, \underline{c}_B includes all the Coriolis/centrifugal/damping term, E_B is the actuation transformation matrix that maps the joint torques to the corresponding independent joint coordinates. The detailed expressions can be found in [25].

B. Dynamics of the NH-WMM

The NH-WMM is constructed by attaching a two-revolute-joint linkage to the WMR at the point P_a . The configuration of the Arm 1 and Arm 2 are parameterized by the absolute joint angles of θ_1 and θ_2 , actuated by τ_1 and τ_2 , respectively, and operates solely in the horizontal plane. The rest of the relevant physical parameters are listed in Table I. The full set of extended generalized coordinates in this case, including the manipulator configuration variables, are $\underline{q}^T = [\underline{q}_B^T \ \underline{q}_M^T] = [x_c \ y_c \ \phi \ \theta_R \ \theta_L \ \theta_1 \ \theta_2]$ and $\underline{q}_M^T = [\theta_1 \ \theta_2]$. The NH-WMM possesses the same set of constraints described

in (1). Hence, the constraint matrix can be extended to:

$$A \dot{\underline{q}} = \underline{0} \quad \text{and} \quad A = \begin{bmatrix} A_B & 0_{3 \times 2} \end{bmatrix} \quad (6)$$

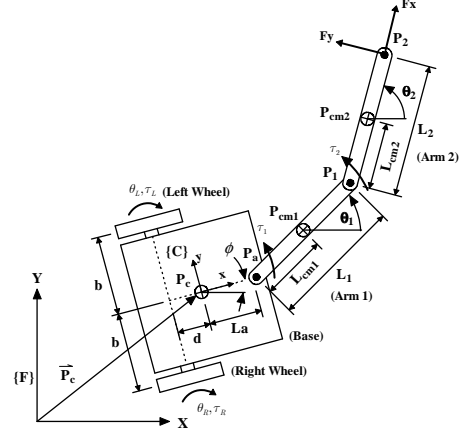


Fig. 2. Nonholonomic wheeled mobile manipulator (NH-WMM) nomenclature

TABLE I
PHYSICAL PARAMETERS OF THE WHEELED MOBILE MANIPULATOR

Parameters	Variables	Values	Units
Mass of the wheel	m_w	0.159	kg
Mass of mobile base	m_c	17.25	kg
Mass of Arm 1	m_1	2.56	kg
Mass of Arm 2	m_2	1.07	kg
Moment of inertia (MI) of the wheels about its center of mass (CM)	I_w	0.0002	kg-m ²
MI of mobile base about its CM	I_c	0.297	kg-m ²
MI of Arm 1 about its CM	I_1	0.148	kg-m ²
MI of Arm 2 about its CM	I_2	0.0228	kg-m ²
Half distance between the two wheels	b	0.182	m
Radii of the wheels	r	0.0508	m
Distance from the center of the wheel axle to the CM of the mobile base	d	0.116	m
Distance from CM of the mobile base to the point P_a	L_a	0.100	m
Length of Arm 1	L_1	0.514	m
Length of Arm 2	L_2	0.362	m

Taking the independent velocities $\underline{\nu}^T = [\underline{\nu}_B^T \ \dot{\underline{q}}_M^T]$, we can similarly determine the null-space matrix S that annihilate the constraint matrix in (6) as:

$$\dot{\underline{q}} = S \underline{\nu} \quad \text{and} \quad S = \begin{bmatrix} S_B & 0_{5 \times 2} \\ 0_{2 \times 2} & I_{2 \times 2} \end{bmatrix} \quad (7)$$

We consider the task-space to be the Cartesian coordinates of the end-effector $\underline{x} = (x_e, y_e)$. The Jacobian relating independent joint velocities to task-velocity can be written as:

$$\dot{\underline{x}} = J \underline{\nu}, \quad J = \begin{bmatrix} J_B & J_M \end{bmatrix} \quad \text{and} \quad J_M = \begin{bmatrix} -L_1 S_1 & -L_2 S_2 \\ L_1 C_1 & L_2 C_2 \end{bmatrix} \quad (8)$$

where $S_l = \sin \theta_l$, $C_l = \cos \theta_l$, $l = 1, 2$. Finally, assume that the constrained dynamics of the NH-WMM is written as:

$$H_C(\underline{q}) \ddot{\underline{q}} + \underline{c}_C(\underline{q}, \dot{\underline{q}}) = E_M \underline{\tau}_M + E_E \underline{F} - A^T \underline{\lambda}, \quad A \dot{\underline{q}} = \underline{0} \quad (9)$$

The *projected reduced dynamics* of the NH-WMM can be then obtained by projection using S^T as:

$$H(\underline{q})\dot{\underline{v}} + \underline{c}(\underline{q}, \underline{v}) = \underline{\tau}(\underline{q}) + \underline{\tau}_E(\underline{q}) \quad (10)$$

where $H = S^T H_C S$ is the inertia matrix, $\underline{c} = S^T (H_C \dot{S} + \underline{c}_C)$ is the Coriolis/centrifugal/damping terms, $\underline{\tau} = S^T E_M \underline{\tau}_M$ is the input torque, and $\underline{\tau}_E = S^T E_E \underline{F}$ is the external forces/torque, all described in the feasible motion space. The derivation of the above matrices is straightforward, and we refer the reader to [21] for the details. Since our system operates in the horizontal plane, there is no gravitational contribution to the dynamics.

III. DECOUPLED TASK- AND NULL-SPACE DYNAMIC CONTROL STRATEGY

The focus of this paper is the experimental validation of a dynamic-level control routine for the NH-WMM that allows for independent dynamic control of both the task-space (external end-effector) and the null-space (internal manipulator DOF). To this end, we adapt dynamic redundancy resolution methods developed for control of serial-chain redundant robots [22, 24] for use with the NH-WMM [21].

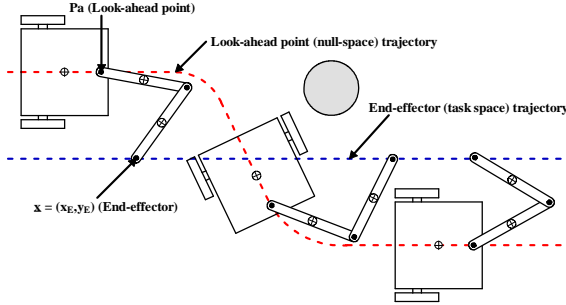


Fig. 3. Wheeled mobile manipulator with alternate specification of desired end-effector and base trajectories

The primary task is assumed to be one of controlling the motion and/or force interactions of the end-effector with the attached payload/external environment. Once the primary end-effector task has been accomplished, the secondary task is assumed to be one of controlling the surplus internal DOF within the system (such as the relative pose of the mobile robot base and arms). In this work, we use the extra configuration redundancy to our advantage by controlling the “look-ahead” point to follow an alternate desired trajectory as depicted in Fig. 3.

In (8), given that $\dot{\underline{x}}$ and \underline{v} are the task-space and independent feasible joint-space velocity vectors, respectively. For a kinematically redundant system, the dimension of \underline{v} is greater than the dimension $\dot{\underline{x}}$. Hence, the general solution for \underline{v} can be written as:

$$\underline{v} = J^\# \dot{\underline{x}} + N \dot{\underline{z}} \quad (11)$$

where $J^\#$ and N are the generalized pseudo-inverse and the null-space of J , respectively, and $N \dot{\underline{z}}$ is the consistent joint-velocity due to the internal motion of the manipulator. A resolved acceleration scheme can be written as:

$$\dot{\underline{v}} = J^\# \ddot{\underline{x}} + \dot{J}^\# \dot{\underline{x}} + N \ddot{\underline{z}} + \dot{N} \dot{\underline{z}} \quad (12)$$

where the first two terms in the RHS are the joint-space

acceleration required to perform the task, and the last two terms represent the consistent joint-space acceleration due to the internal motion. In the resolved *force* system, the relationship between the task forces \underline{F} and the joint forces $\underline{\tau}$ can be similarly written as:

$$\underline{\tau} = J^T \underline{F} + N^T \underline{\tau}_z \quad (13)$$

where $N^T = I - J^T J^{\#T}$ projects the arbitrary (internal) joint torques $\underline{\tau}_z$ to the null-space of J^T to provide consistent manipulator motion. However, the pseudo-inverse $J^\#$ might not be “consistent” with the dynamic of the manipulator. Hence, we define a weighted pseudo-inverse of J by the inverse of the manipulator inertia matrix H^{-1} as:

$$\bar{J} = J_{H^{-1}}^\# = H^{-1} J^T (J H^{-1} J^T)^{-1} \quad (14)$$

and the corresponding null-space as:

$$\bar{N} = I - \bar{J} \quad (15)$$

Such an *inertia-matrix weighted pseudoinverse* has geometric significance since it endows the final task space with a kinetic-energy metric defined on the tangent space of a selected manipulator [23]. As noted in [24], the use of such dynamically consistent pseudoinverse simplifies the process of decoupling the task- and null-space dynamics. Premultiplying both sides of (10) by $I = J^T \bar{J}^T + \bar{N}^T$, substituting (12) and (13) into (10) yields:

$$J^T \underline{F} + N^T \underline{\tau} = \Upsilon_1 + \Upsilon_2 + \Upsilon_3 \quad (16)$$

$$\Upsilon_1 = J^T J^{\#T} [H J^\# (\ddot{\underline{x}} - \dot{J} \dot{\underline{x}}) + \underline{c} - \underline{\tau}_E]$$

$$\Upsilon_2 = N^T (H N \ddot{\underline{z}} + \underline{c} - \underline{\tau}_E)$$

$$\Upsilon_3 = J^T J^{\#T} H N \ddot{\underline{z}} + N^T H J^\# (\ddot{\underline{x}} - \dot{J} \dot{\underline{x}})$$

In (16), Υ_1 filters the overall dynamics using $J^T J^{\#T}$ to allow only the task-space dynamics to pass through. Likewise, Υ_2 uses N^T to retain the null-space component of the combined dynamics. Υ_3 includes all the cross-coupling dynamic terms and becomes identically *zero* when the dynamically consistent pseudo-inverse is employed. Thus, taking $J^\# = \bar{J}$ and $N = \bar{N}$, the final EOM can be expressed in the task-space as:

$$M(\underline{q})\dot{\underline{u}} + \underline{\mu}(\underline{q}, \underline{u}) = \underline{F} + \underline{F}_E \quad (17)$$

where $M = \bar{J}^T H \bar{J} = (J H^{-1} J^T)^{-1}$ is the apparent inertia matrix, $\underline{\mu} = \bar{J}^T \underline{c} - M \dot{J} \underline{u}$ is the apparent Coriolis/centrifugal/damping terms, $\underline{F} = \bar{J}^T \underline{\tau}$ is the apparent input force, and $\underline{F}_E = \bar{J}^T \underline{\tau}_E$ is the apparent external force, all described in the task-space. The control input that decouples the task- and null-space can then be defined as:

$$\underline{\tau} = J^T M(\underline{u} - \dot{J} \underline{u}) + \bar{N}^T H(\underline{v} + \dot{J} \underline{u}) + \underline{\mu} + J^T \underline{F}_E \quad (18)$$

where \underline{u} and \underline{v} are the new control inputs to the task- and null-space, respectively. After substituting (18) into (16) and simplifying, the final equivalent controlled closed loop dynamics in the independent task- and null-spaces may be

written, respectively, as:

$$\underline{u} - \ddot{\underline{x}} = \underline{0} \quad \text{and} \quad \underline{v} - \dot{\underline{v}} + \dot{J}\dot{\underline{x}} = \underline{0} \quad (19)$$

We note that due to the explicit performance of nonlinear feedback linearization, the two subspace dynamics correspond to those of equivalent linear systems. Hence for the *task-space*, we select an impedance controller [27]:

$$\underline{u} = \ddot{\underline{x}}^d + K_V \dot{\underline{e}} + K_P \underline{e} + K_F (\underline{F}_E^d - \underline{F}_E) \quad (20)$$

where the superscript d indicates the desired quantities; $\underline{e} = \underline{x}^d - \underline{x}$, $\dot{\underline{e}} = \dot{\underline{x}}^d - \dot{\underline{x}}$ are the end-effector position and velocity errors, respectively; K_V , K_P , and K_F are positive definite constant matrices (to maintain stability); and \underline{F}_E^d is the desired end-effector force which creates the closed-loop task-space behavior of a second-order spring-damper-mass system with a driving force determined by the desired impedance as:

$$\ddot{\underline{e}} + K_V \dot{\underline{e}} + K_P \underline{e} = -K_F (\underline{F}_E^d - \underline{F}_E) \quad (21)$$

where $\ddot{\underline{e}} = \ddot{\underline{x}}^d - \ddot{\underline{x}}$ is the acceleration errors. The selection of the control gains can now be done by appropriate linear pole-placement techniques. In this paper, we consider $\underline{F}_E^d = \underline{0}$ and \underline{F}_E is an “external disturbance force” at the end-effector. However, this can be extended to the case with force regulation, and a preliminary simulation study has been reported in [21]. Finally, it is noted that such a nonlinear feedback linearization allows one to explicitly cancel the nonlinearities and replace the original dynamics with an (exact) linearized dynamical system. Such a model-based controller design tends to be dependent on accurate dynamic modeling. However, as noted in [28], even in the absence of a model, PD control with gravity compensation, is sufficient to ensure point stabilization (and even permits tracking albeit with some lag). Hence, inadequate modeling here would allow a graceful but stable degradation of the performance during the transition from the completely linearized (computed torque) case to the uncompensated (unmodeled) case.

IV. NULL SPACE CONTROLLERS

Due to the decoupled nature, the selection of null-space controllers does not affect the task space performance. Here, we examine the use of kinematic and dynamic tracking algorithms for the look-ahead point on WMR as two alternatives for the null-space controllers. Obstacle-avoidance methods using potential fields/navigation functions [29] or combined with other trajectory-following methods [30] are viable alternatives. However, by affecting the internal configuration dynamics, the selection can significantly alter the required control effort as we will discuss further later in the detailed case studies.

In the first case, a *kinematic controller* for the WMR is derived from the kinematic equations in (4). As long as the look-ahead point does not coincide with the midpoint of the wheel axle ($L_a \neq -d$), J_B is nonsingular. Hence the wheel velocities \underline{v}_B can be determined from the velocity of the look-

ahead point as:

$$\underline{v}_B = J_B^{-1} \dot{\underline{x}}_B \quad (22)$$

This can be extended to factor in a closed-loop Cartesian error dynamic for the look-ahead point as:

$$\underline{v}_B = J_B^{-1} [\dot{\underline{x}}_B^d + K_{PB} (\underline{x}_B^d - \underline{x}_B)] \quad (23)$$

where \underline{x}_B^d and $\dot{\underline{x}}_B^d$ are the desired position and velocity of the look ahead point, respectively. It is straightforward to see that this error dynamic is stable when K_{PB} is positive definite. These desired wheel velocities can be given as set points to a rate controller for a kinematically controlled motor or backstepped to provide inputs to a torque-controlled motor.

In the second case, we choose the dynamic tracking algorithm presented in [25] to achieve input-output linearization and input-output decoupling. In our case, choosing the look-ahead point to be the output of the system is corresponding to the Type I output. The necessary and sufficient condition for input-output linearization for the proposed choice of outputs is that the decoupling matrix has full rank. Thus, similarly, the only singularity occurs when the look-ahead point coincides with the midpoint of the wheel axle. Using the dynamic equation in (5), the nonlinear feedback $\underline{\tau}_B = E_B^{-1} [H_B \eta_B + \underline{c}_B]$, and a change of input $\underline{\eta} = J_B^{-1} (\underline{\xi} - \dot{J}_B \underline{\nu})$, the linearized and decoupled system can be converted to $\ddot{\underline{x}}_b = \underline{\xi}$, whose controller is designed using standard linear control techniques.

V. IMPLEMENTATION FRAMEWORK

We examine the design and development of an implementation framework that emphasizes both virtual prototyping (VP) based refinement and hardware-in-the-loop (HIL) experimentation, shown in Fig. 4(a).

A. Virtual prototyping based refinement

In the first stage, we employ virtual prototyping (VP) tools to rapidly create, evaluate and refine parametric models of the overall system and test various algorithms in simulation within a virtual environment. Simplified solid model of the WMR and the manipulator of interest are created in SolidWorks, and exported with the corresponding geometric and material properties into visualNastran Desktop 4D (vN4D), an MCAE tool that allows physics-based simulation of dynamic systems. Fig. 4(a) shows an example of the application of such framework for simulating the NH-WMM controlled by an algorithm implemented in Simulink. State information (positions/velocities) and control-input information (torques/forces) are exchanged at every time-step in this co-simulation approach. However, the utility of such virtual testing is limited by: (a) the ability to correctly model and simulate the various phenomena within the virtual environment; (b) the fidelity of the available simulation tools; and ultimately, (c) the ability of the designer to correctly model the desired system and suitably interpret the results.

B. Hardware-in-the-loop experimentation

We employ a *hardware-in-the-loop* (HIL) methodology for rapid experimental verification of the real-time controllers on the electromechanical mobile manipulators prototypes. We opted to create a physical NH-WMM system [shown in Fig. 1(b)] from scratch due to the flexibility it offered over retrofitting an off-the-shelf WMR base with an off-the-shelf manipulator arm. The additional dynamic bandwidth obtained by use of high-performance components is especially pertinent to our anticipated use of the NH-WMMs for active force-redistribution during cooperative payload manipulation tasks.

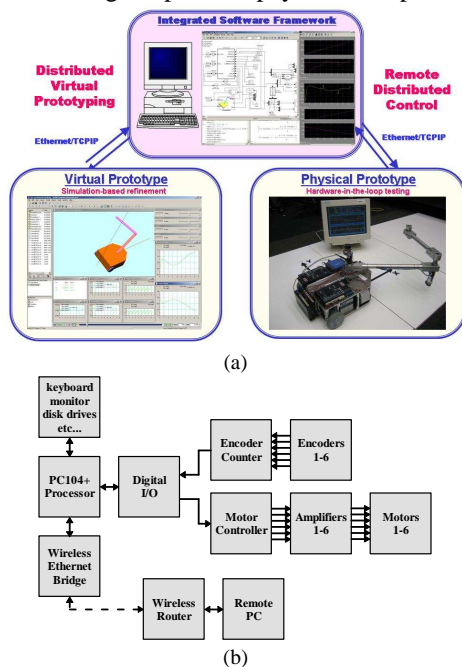


Fig. 4. (a) The two stage implementation framework emphasizes virtual prototyping and hardware-in-the-loop physical testing, and (b) the flowchart summarizing signal and power flow interactions of the electronic hardware.

The NH-WMM is constructed using two geared motor powered wheels and one passive MECANUM-type casters. A passive MECANUM-type front caster is preferred (over a conventional wheel casters) to eliminate any constraints on the maneuverability. The mounted manipulator arm has two active revolute joints with axes of rotation parallel to each other and perpendicular to the mobile platform (and the ground). The first joint can be placed anywhere along the mid-line on top frame of the platform at a distance $L_u = d + L_a$ from center of the wheel axle (see Fig. 2). The end-effector is a flat plate supported by a passive revolute joint that ensures that no moment can be transferred to the manipulator. Each of the two joints is instrumented with an optical encoder that can measure the joint rotations and has a DC motor attached. Independent lead-acid batteries provide power supplies for the actuator systems and the electronic-controllers. The complete assembled two-link mobile manipulator is shown in Fig 1(b).

A PC/104 system equipped with an xPC Target Real-Time Operating System (RTOS) serves as the embedded controller. A PC104+ embedded computer (VersaLogic EPM-CPU-3 133MHz 32-bit processor) is used to perform all the onboard

high-level processing, control and communication. A custom Atmel-based encoder counter circuit board is constructed for the purpose of reading up to six quadrature encoders that can store the position of each encoder with a 32-bit integer variable and asynchronously sends this data to the PC104. Similarly, a custom Atmel-based motor-controller circuit board is constructed for the purpose of providing a PWM reference signal to six current controlled power amplifiers. A digital I/O card (Diamond Systems Garnet MM) serves to provide a buffered bi-directional digital interface between the PC/104 system and the custom circuit boards. Commercial-off-the-shelf current amplifiers (Maxon 4Q-DC brush DC 5A amplifier) are used to generate drive currents proportional to the reference voltage for the motors. The flow chart in Fig 4 (b) summarizes the signal and power-flows interactions to control the system.

The embedded PC/104 controller communicates with a designated host computer using TCP/IP for program download and data logging. The host computer with MATLAB/Simulink/Real Time Workshop provides a convenient GUI environment for system-level software development using a block-diagrammatic language. The compiled executable is downloaded over the network and executed in real-time on the embedded controller while accessing locally installed hardware components. In particular, the ability to selectively test components/systems at various levels (e.g. individual motors/encoders, individual WMR bases or entire NH-WMMs) without wearing out components during design iterations is proven to be very useful. Numerous calibration, simulation and experimental studies carried out with this framework are reported in [31].

VI. CASE STUDIES

The desired trajectories used in the case-studies are representative examples of tasks prescribed for the NH-WMM (see Fig. 3). The primary task is the requirement for the end-effector to track a wide variety of task-space trajectories (time-indexed straight-lines, sinusoids and circles). Secondly, we require the look-ahead point on the WMR base to follow a desired trajectory as closely as possible (when not in direct conflict with the primary task). The desired WMR trajectories are not limited to only feasible trajectories – but now include straight-line, sinusoidal and circular trajectories. The dynamic redundancy-resolution framework naturally prioritizes the tracking of the end-effector trajectory over the look-ahead point at execution time. In these case studies, we examine how the system is able to: (a) dynamically correct for initial errors in the required trajectory; (b) accommodate the external force disturbance by an internal configuration change exploiting the redundancy; and (c) detect and correct these internal configuration changes back to the preferred overall configuration. We pay particular attention to the required torque inputs to the right and left wheels of the WMR to highlight the importance of suitable selection of null-space controllers as well as appropriate actuation selection during the

construction of the electromechanical system.

A. Case I: Simple trajectory tracking

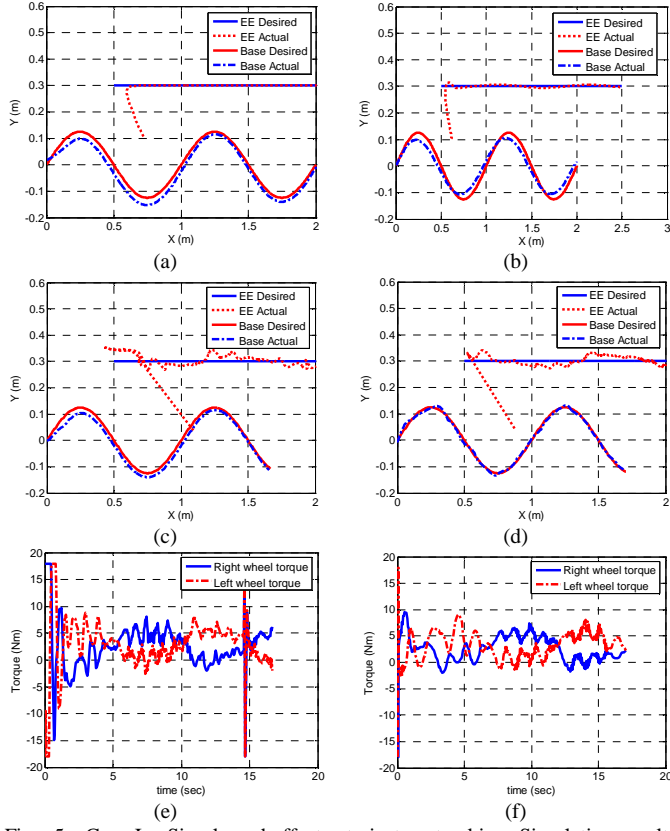


Fig. 5. Case I – Simple end-effector trajectory tracking: Simulation results using (a) kinematic and (b) dynamic controllers for the look-ahead point tracking. (c) and (d) are the corresponding experimental tracking results. (e) and (f) are required wheel torque profiles for the kinematic and dynamic controllers, respectively.

In the first case study, we show the capability of the system to: (a) correct the initial errors, (b) track the desired trajectories, and (c) prioritize the primary task. We also highlight the performance between the different controllers implemented described in the previous section. The desired end-effector trajectory is a straight line of $x_e^d(t) = (0.1t + 0.5)m$, $y_e^d(t) = 0.3m$ and the desired look-ahead point trajectory $\underline{x}_B^d(t)$ is a sinusoid of $x_a^d(t) = (0.1t)m$, $y_a^d(t) = 0.125 \sin(0.2\pi t)m$. Fig. 5(a) and (b) show the simulation results when the look-ahead point are kinematically and dynamically controlled in the null-space, respectively. In both cases, it can be seen that the initial error of the end-effector trajectories are corrected and being tracked very closely within a small transient. However, the look-ahead point is tracked as closely as possible, but with errors relatively larger than the end-effector tracking, which progressively reduced. The controller is able to prioritize the primary task of end-effector tracking, while attempting to achieve the secondary task of look-ahead point tracking as close as possible. Fig. 5(c) and (d) show the corresponding successful hardware experimental tracking results that reflect the similar behavior. However, the overall required input

torques to the right and left wheels are smoother/lower when the dynamic controller is employed [see Fig. 5(f)] than for the kinematic controller case [see Fig. 5(e)]. Thus, the hardware requirements (bandwidth and peak capacity of actuators and affiliated electronics) can be significantly different based on selection of the null-space controller (despite the comparable primary task tracking performance). This is a critical consideration for selection/design of mechatronics system and is not often adequately discussed in the literature. We also note that model parameter uncertainties critically affect control performance – detailed sensitivity studies are reported in [31].

B. Case II: Disturbance detection and rejection

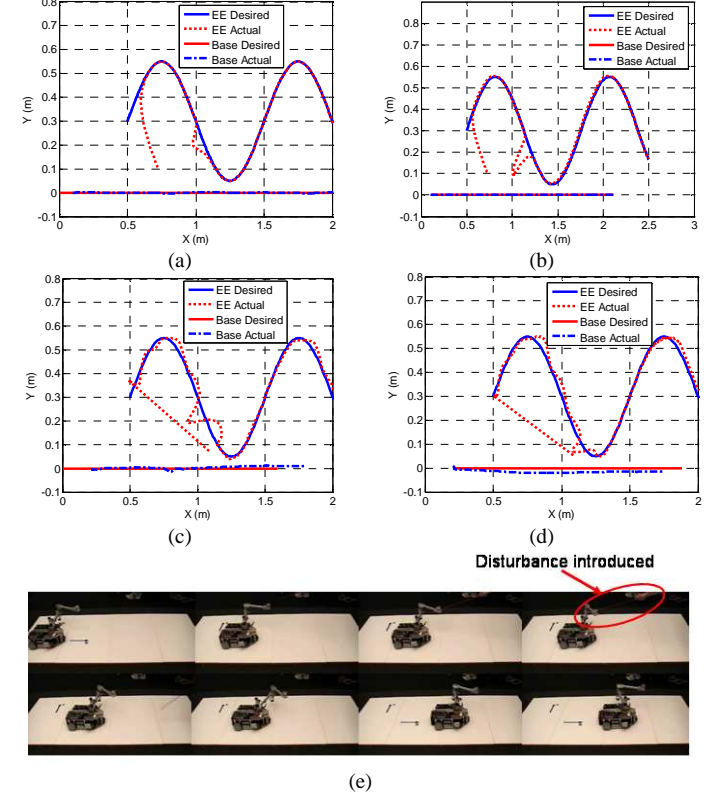


Fig. 6. Case II – Disturbance detection and rejection: Simulation results using (a) kinematic and (b) dynamic controllers for the look-ahead point tracking. (c) and (d) are the corresponding experimental tracking results. (e) Screenshots showing the introduction of disturbance to the physical NH-WMM when moving from left to right. The frame sequence is from left to right, and from first row to second row.

In the second case study, we examine the capability of the system to: (a) accommodate the disturbance due to external force by internal configuration change, and (b) subsequently correct for the deviations. The desired end-effector trajectory is $x_e^d(t) = (0.1t + 0.5)m$, $y_e^d(t) = 0.3 + 0.25 \sin(0.2\pi t)m$ and the desired look-ahead point trajectory is a straight line of $x_a^d(t) = (0.1t)m$, $y_a^d(t) = 0m$. We intentionally introduce an external disturbance force to the end-effector when the system is tracking the desired trajectories. Fig. 6(a) and (b) depict the simulation results of tracking of the end-effector position and the look-ahead point using the kinematic and dynamic controller in the null-space, respectively. The

(impulsive) disturbance force of $(F_x, F_y) = (-0.3, -0.2) N$ is introduced at the time $t = 5.5s$ at the end-effector. We can see that the kinematic controller responds aggressively to bring the system back to achieve accurate tracking. However, dynamic controller has a more graduated/softer response allowing for some transients before coming back to the accurate tracking. This is also reflected in the experimental implementation results seen in Fig 6(c) and (d) for the kinematic and dynamic null-space controllers, respectively. While we cannot provide accurate disturbance as in the simulation case, we introduce the disturbance to the system in the form of poking using a steel rod at the end-effector [see screenshots in Fig 6(e)]. We did not co-locate the initial configuration of the end-effector with the desired one, hence the system first accounts for the initial error. Subsequently, while tracking the system was able to accommodate the disturbance and detect it through the system configuration change measured by the joint encoders and correct for it.

C. Case III: Circular trajectory with competing criteria

In the third case study, we show the capability of the system to: (a) track competing primary/secondary tasks, and (b) prioritize the primary task. The task of tracking the look-ahead point trajectory sometimes tends to suffer due to inconsistency with the nonholonomic constraints of the WMR. This would normally then affect the primary end-effector tracking performance as well. However, the results of this study depict the ability of the controller to prioritize the primary task and ensure its performance.

The desired end-effector trajectory is the inner circle $x_e^d(t) = 0.3 \sin(0.1\pi t) m$, $y_e^d(t) = 0.7 + 0.3 \cos(0.1\pi t) m$ and the desired look-ahead trajectory is the outer circle $x_a^d(t) = 0.7 \sin(0.1\pi t) m$, $y_a^d(t) = 0.7(1 + \cos(0.1\pi t)) m$. Both circles are traversed in the clockwise direction with nominal initial position for end-effector as $(0.0, 1.0) m$ and for look-ahead point as $(0.0, 1.4) m$. We first present the simulation results using the kinematic and dynamic null-space controllers in Fig. 7(a) and (b), respectively. Note that the initial location of the look-ahead point is offset radially by $0.15m$ from the desired circular trajectory (but with forward motion along the tangential direction). Thus, the base is unable to (immediately) compensate for the offset due to the nonholonomic constraint.

Although desired trajectories are conflicting, the system successfully achieves the primary end-effector tracking task closely while attempting to realize the secondary task as closely as possible. As seen in Fig. 7(a)-(b), the look-ahead point converges to the desired circular trajectory within one full traversal of the circle, even for an exaggerated initial offset. Similar trends are seen with the hardware experimental results in Fig. 7(c) and (d) using kinematic and dynamic null-space controllers respectively, albeit with smaller offsets to avoid actuator saturation effects. We again investigate the input torque profile to the right and left wheels in Fig. 7(e) and

(f), where kinematic and dynamic null-space controllers are implemented, respectively. It is again noteworthy that the input torques in the kinematic case are much more “aggressive” than the dynamic case.

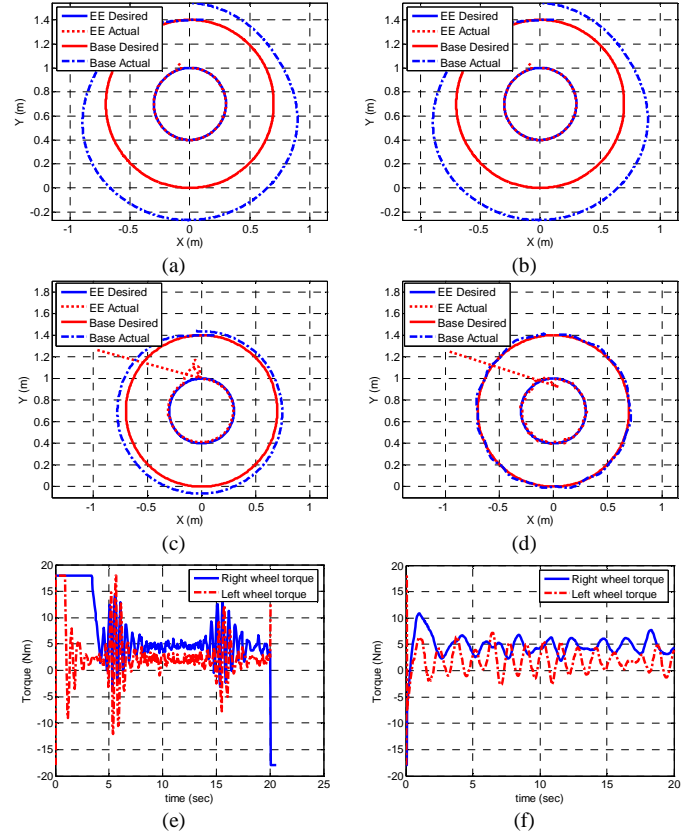


Fig. 7. Case III – Circular trajectory with competing criteria: Simulation results using (a) kinematic and (b) dynamic controllers for the look-ahead point tracking. (c) and (d) are the corresponding experimental tracking results. (e) and (f) are required wheel torque profiles for the kinematic and dynamic controllers, respectively.

VII. DISCUSSION AND CONCLUSION

The coupling of the nonholonomic base constraints with the inherent redundancy in NH-WMMs creates significant challenges for control of end-effector (motion/force) interactions. Thus, the focus of this paper was the development of a dynamic-level redundancy-resolution strategy for such NH-WMMs. The primary task was assumed to be one of controlling the motion and/or force interactions of the end-effector with respect to the attached payload/external environment. The secondary task is assumed to be one of controlling the surplus (internal) DOF within the system (relative pose of the mobile base) and sought to be achieved only upon satisfaction of the primary task. Such a systematic approach to resolution of the redundancy while allowing for internal reconfiguration is key to many of the current and envisaged applications for such systems. At the outset, the results verified that the capability of the developed control framework to resolve redundancy and permit creation of a decoupled end-effector impedance-mode controller. Furthermore, by virtue of the nonlinear feedback linearization, any desired task-space behavior (specified in terms of damping

ratio, natural frequency, time constant) may be prescribed and realized for end-effector. The results also demonstrate the ability to exploit the redundancy to simultaneously follow various end-effector trajectory primarily and look-ahead point trajectory of WMR secondarily (with a natural prioritization to end-effector tracking performance). This was studied in simulation using virtual prototypes and subsequently hardware experiments on physical electromechanical prototype. Finally, two variants of null-space controllers were deployed and it can be observed that the kinematic version was more aggressive than the dynamic version. In order to better realize the systems in the hardware level, the dynamic version might be favorable. Future works include using an independent force-sensor to determine the ability to regulate end-effector forces.

REFERENCES

- [1] B. Bayle, J.-Y. Fourquet, and M. Renaud, "Manipulability of Wheeled Mobile Manipulators: Application to Motion Generation," *International Journal of Robotics Research*, vol. 22, pp. 565-581, 2003.
- [2] Y. Yamamoto and X. Yun, "Coordinating Locomotion and Manipulation of a Mobile Manipulator," *IEEE Transactions on Automatic Control*, vol. 39, pp. 1326-1332, 1994.
- [3] S. A. Velinsky and J. F. Gardner, "Kinematics of mobile manipulators and implications for design," *Journal of Robotics Systems*, vol. 17, pp. 309-320, 2000.
- [4] H. Seraji, "A Unified Approach to Motion Control of Mobile Manipulators," *The International Journal of Robotics Research*, vol. 17, pp. 107-118, February 1998.
- [5] M. Fruchard, P. Morin, and C. Samson, "A Framework for the Control of Nonholonomic Mobile Manipulators," *International Journal of Robotics Research*, vol. 25, pp. 745-780, 2006.
- [6] A. De Luca, G. Oriolo, and P. R. Giordano, "Image-based Visual Servoing Schemes for Nonholonomic Mobile Manipulators," *Robotica*, vol. 25, pp. 131-145, March/April 2007.
- [7] J. Park and O. Khatib, "A Haptic Teleoperation Approach Based on Contact Force Control," *International Journal of Robotic Research*, vol. 25, pp. 575-591, May - June 2006.
- [8] C. P. Tang, R. M. Bhatt, M. Abou-Samah, and V. Krovi, "A Screw-Theoretic Analysis Framework for Payload Transport by Mobile Manipulator Collectives," *IEEE/ASME Transactions on Mechatronics*, vol. 11, pp. 169-178, April 2006.
- [9] G. Campion, G. Bastin, and B. D'Andrea-Novet, "Structural Properties and Classification of Kinematic and Dynamic Models of Wheeled Mobile Robots," *IEEE Transactions on Robotics and Automation*, vol. 12, pp. 47-62, February 1996.
- [10] Y. Nakamura, *Advanced Robotics: Redundancy and Optimization*. California: Addison-Wesley Publishing Company, Inc., 1991.
- [11] C.-C. Wang and V. Kumar, "Velocity Control of Mobile Manipulators," in *1993 IEEE International Conference on Robotics and Automation*, 1993, pp. 713-718.
- [12] V. Kumar and K. J. Waldron, "Force distribution in walking vehicles on uneven terrain," *ASME Journal of Mechanisms, Transmissions, and Automation in Design*, vol. 112, pp. 90-99, 1990.
- [13] J. Kerr and B. Roth, "Analysis of Multifingered Hands," *The International Journal of Robotics Research*, vol. 4, pp. 3-17, 1986.
- [14] X. Yun and V. Kumar, "An approach to simultaneous control of trajectory and interaction forces in dual arm configurations," *IEEE Transactions on Robotics and Automation* vol. 7, pp. 618-625, 1991.
- [15] W. Gueaieb, F. Karray, and S. Al-Sharhan, "A Robust Hybrid Intelligent Position/Force Control Scheme for Cooperative Manipulators," *IEEE/ASME Transactions on Mechatronics*, vol. 12, pp. 109-125, April 2007.
- [16] X. Zhu, G. Tao, B. Yao, and J. Cao, "Adaptive Robust Posture Control of Parallel Manipulator Driven by Pneumatic Muscles With Redundancy," *IEEE/ASME Transactions on Mechatronics*, vol. 13, pp. 441-450, August 2008.
- [17] Y. Yamamoto and X. Yun, "Effect of the Dynamic Interaction on Coordinated Control of Mobile Manipulators," *IEEE Transactions on Robotics and Automation*, vol. 12, pp. 816-824, 1996.
- [18] J. Y. Lew and S.-M. Moon, "A Simple Active Damping Control for Compliant Base Manipulators," *IEEE/ASME Transactions on Mechatronics*, vol. 6, pp. 305-310, September 2001.
- [19] J. Tan, N. Xi, and Y. Wang, "Integrated Task Planning and Control for Mobile Manipulators," *The International Journal of Robotics Research*, vol. 22, pp. 337-354, 2003.
- [20] F. Inoue, T. Murakami, and K. Ohnishi, "A Motion Control of Mobile Manipulator with External Force," *IEEE/ASME Transactions on Mechatronics*, vol. 6, pp. 137-142, June 2001.
- [21] G. D. White, R. M. Bhatt, and V. N. Krovi, "Dynamic Redundancy Resolution in a Nonholonomic Wheeled Mobile Manipulator," *Robotica*, vol. 25, pp. 147-156 March 2007.
- [22] O. Khatib, "A Unified Approach to Motion and Force Control of Robot Manipulators: The Operational Space Formulation," *IEEE Journal on Robotics and Automation*, vol. RA-3, pp. 43-53, 1987.
- [23] F. Bullo and A. D. Lewis, *Geometric Control of Mechanical Systems: Modeling, Analysis and Design for Simple Mechanical Control Systems*. New York NY: Springer-Verlag, 2004.
- [24] B. Nemeec and L. Zlajpah, "Force Control of Redundant Robots in Unstructured Environment," *Industrial Electronics, IEEE Transactions on*, vol. 49, pp. 233-240, February 2002.
- [25] N. Sarkar, X. Yun, and V. Kumar, "Control of Mechanical Systems With Rolling Constraints: Application to Dynamic Control of Mobile Robots," *International Journal of Robotic Research*, vol. 13, pp. 55-69, February 1994.
- [26] C. B. Low and D. Wang, "GPS-Based Tracking Control for a Car-Like Wheeled Mobile Robot With Skidding and Slipping," *IEEE/ASME Transactions on Mechatronics*, vol. 13, pp. 480-484, August 2008.
- [27] R. Anderson and M. Spong, "Hybrid impedance control of robotic manipulation," *IEEE Journal of Robotics and Automation* vol. 4, pp. 549-556 1988.
- [28] J. Slotine, Li, W., *Applied Nonlinear Control*. New Jersey: Prentice Hall, 1991.
- [29] H. Choset, K. M. Lynch, S. Hutchinson, G. Kantor, W. Burgard, L. E. Kavraki, and S. Thrun, *Principles of Robot Motion - Theory, Algorithms, and Implementation*. Cambridge MA: MIT Press, 2005.
- [30] C.-L. Hwang and L.-J. Chang, "Trajectory Tracking and Obstacle Avoidance of Car-Like Mobile Robots in an Intelligent Space Using Mixed H₂/H_∞ Decentralized Control," *IEEE/ASME Transactions on Mechatronics*, vol. 12, pp. 345-352, June 2007.
- [31] R. M. Bhatt, "Towards Modular Cooperation between Multiple Nonholonomic Mobile Manipulators," in *Dept. of Mechanical & Aerospace Engineering*. vol. PhD Buffalo: University at Buffalo, 2007.

Glenn D. White is currently a Project Engineer in General Motors, Honeoye Falls NY. He received the B.S. and M.S. degrees in Mechanical Engineering in 2004 and 2006, respectively, both from the University at Buffalo. His research interest is mechatronics designs of mobile robots.

Rajankumar Bhatt (S'02-M'07) is currently an assistant research engineer at The University of Iowa's Virtual Soldier Research (VSR) program. He received the M.S. and Ph.D. degrees in mechanical engineering in 2004 and 2007, respectively, from the University at Buffalo, and the B.E. in mechanical engineering in 2001 from the MS University of Baroda, India. His research interest is in control of mobile manipulators.

Chin Pei Tang (S'02) is currently a Ph.D. candidate in Department of Mechanical and Aerospace Engineering in University at Buffalo. He received the B.S. and M.S. degree in Mechanical Engineering in 2002 and 2004 respectively. His research interest is in cooperative mobile robots.

Venkat Krovi (S'97-M'99) received the M.S. and Ph.D. degrees from the University of Pennsylvania, Philadelphia, in 1995 and 1998, respectively, both in mechanical engineering. In 2001, he joined the Department of Mechanical and Aerospace Engineering, University at Buffalo. His research interests include design, analysis, and prototyping of novel articulated mechanical systems. He was the recipient of the 2004 National Science Foundation CAREER Award.